Fluid Phase Equilibria 353 (2013) 101–114

Contents lists available at SciVerse ScienceDirect

Fluid Phase Equilibria

journal homepage: www.elsevier.com/locate/fluid

Fast and robust algorithm for calculation of two-phase equilibria at given volume, temperature, and moles

Tereza Jindrová, Jiří Mikyška*

Czech Technical University in Prague, Faculty of Nuclear Sciences and Physical Engineering, Department of Mathematics, Trojanova 13, 120 00 Prague 2, Czech Republic

ARTICLE INFO

Article history:
Received 21 January 2013
Received in revised form 29 May 2013
Accepted 30 May 2013
Available online 14 June 2013

Keywords:
Two-phase equilibrium
Constant volume flash
Helmholtz free energy minimization
Newton–Raphson method
Modified Cholesky factorization

ABSTRACT

We develop a new algorithm for the calculation of phase splitting at constant volume, temperature, and moles. The method is based on the direct minimization of the total Helmholtz free energy of the mixture with respect to the mole- and volume-balance constraints. The algorithm uses the Newton–Raphson minimization method with line-search and modified Cholesky factorization of the Hessian to produce a sequence of states with decreasing values of the total Helmholtz free energy. The algorithm is initialized using an initial guess that is constructed using the results of the constant volume stability testing. The speed and robustness of the algorithm are demonstrated by a number of examples of two-phase equilibrium calculations.

1. Introduction

Consider a closed system of given volume V containing a mixture of n components with mole numbers $N_1,\ldots,N_n$ at temperature T. The goal is to find out if the system is in single phase or splits into phases. If phase splitting occurs, we want to establish composition, densities, and amount of the phases, and eventually, find the equilibrium pressure. The problem of computation of phase equilibria under constant volume, temperature, and moles (the so-called *VT*-flash) is an alternative to the traditional formulation of phase equilibria at constant pressure, temperature, and chemical composition (the so-called *PT*-flash), which has been used in many applications [1–3]. Although the possibility of using alternative variables specifications has been known for a long time, in most applications *PT*-flash has been used to solve the phase equilibrium. To compute phase equilibria under different variables specifications (including *VT*, *PS*, and *PH*), Michelsen [1–4] suggested to use the *PT*-flash algorithm iteratively, trying to find input temperature T and pressure P for the *PT*-flash such that the resulting specification variable (volume V, entropy S, or enthalpy H, respectively) attains the prescribed value. This approach was used in [5] to find the conditions of thermodynamic equilibrium in systems subject to gravitational fields and in [6] to study segregation in centrifugal fields. While this approach allows to reuse existing implementations of *PT*-flash, it is not computationally efficient because many solutions of the *PT*-flash are needed before the equilibrium pressure is found. Another limitation of this approach is that for a pure substance at the saturation pressure, volume is ambiguous (see Example 1 below), and therefore, the nested loop approach must fail to provide correct volume fractions of the split phases. Although the single-component case seems to be a trivial exception, we aim to develop a method that performs equally well for pure substances and mixtures. This motivates our interest in *VT*-based formulation and direct minimization of the total Helmholtz free energy A.

Compared to *PT*-flash, the *VT*-based algorithms for the flash calculation and stability testing have been discussed rarely in the literature. Cabral et al. [7] use the direct minimization of the Helmholtz free energy in problems with various bulk and adsorbed phases. In the *VT*-flash, pressure can become negative during the course of iterations. For this reason, Cabral et al. [7] have evaluated the logarithms of fugacities and pressures using the complex arithmetic. In the *VT*-formulation presented in this paper, the use of complex arithmetic is avoided. This is achieved by expressing the differences of the chemical potentials using the logarithms of volume functions rather than fugacities. The framework of volume functions was developed recently [9] to replace fugacities in the *VT*-based formulations. The first algorithm for the direct calculation of *VT*-flash [9] using the new framework was based on solving the equations of phase equilibria using the succesive substitution iterations (SSI). Numerical examples in [9] demonstrate that the direct calculation of *VT*-flash using SSI can be performed in essentially the same number of iterations as SSI requires in *PT*-flash if applied at the equilibrium pressure. As this pressure is usually not known a-priori

* Corresponding author. Tel.: +420 224358553.
E-mail address: jiri.mikyska@fjfi.cvut.cz (J. Mikyška).

0378-3812/$ – see front matter © 2013 Elsevier B.V. All rights reserved.
http://dx.doi.org/10.1016/j.fluid.2013.05.036

List of notation

Symbol	
A	Helmholtz free energy
b_i	Covolume parameter of the Peng–Robinson EOS
c	Molar concentration
δ_{X-Y}	Binary interaction coefficient between components X and Y
i, j	Component indices
k	Iteration index
μ_i	Chemical potential of the ith component
$M_{w,i}$	Molar weight of the ith component
n	Number of components
N_i	Mole number of the ith component
ω_i	Accentric factor of the ith component
P	Pressure
$P_{i,crit}$	Critical pressure of the ith component
R	Universal gas constant
T	Absolute temperature
$T_{i,crit}$	Critical temperature of the ith component
V	Total volume of the system
z_i	Overall mole fraction of the ith component

(actually, it is one of the results of the *VT*-flash problem), iterative version of the *PT*-flash would require more CPU-time to solve the *VT*-flash problem. Besides its efficiency, there are also other advantages of the *VT*-flash formulation over the *PT*-formulation [11] stemming from the fact that *VT* are the natural variables of pressure-explicit equations of state:

1 As volume is specified and pressure is computed from the equation of state, there is no need to invert the equation of state.
2 As the equation of state is not inverted, the problem of multiple roots of the equation of state is avoided.
3 The algorithm can describe phase splitting in the mixtures as well as in pure components (we will show a specific example of this issue later in this paper).

Although the SSI-algorithm for *VT*-flash works well in many cases, there are several issues to resolve. First, for some problems the SSI algorithm requires too many iterations to converge. Second, if SSI does converge, it does not have to converge to a state corresponding to (at least) a local minimum of the total Helmholtz free energy A. We have found examples, in which the iterates in the SSI-algorithm converge to a state corresponding to the saddle point of A rather than to the point of a minimum of A. In some cases, SSI can converge to the trivial solution although the system should be in two-phase. Providing good initial guesses for the SSI algorithm is another challenge. We have found an example of a binary mixture, for which the iterates in the SSI method diverged from the vicinity of the global minimum of A no matter how close was the initial guess to the point of the global minimum. Recently, we have developed a fast and robust method for testing single-phase stability under constant V and T conditions [10]. This algorithm tests if a small volume of a trial phase with arbitrary density and composition can be split from the initial phase so that the total Helmholtz free energy of the 2-phase system is lower than the energy of the hypothetical single-phase system. If the mixture is stable, the *VT*-flash calculation is avoided. If the mixture splits into phases, the *VT*-stability provides concentrations of a trial phase, which, if taken in a sufficiently small amount from the initial phase, leads to a two-phase system with lower value of A than the hypothetical single phase state. However, the SSI algorithm breaks down if the initial guess from *VT*-stability is used.

To resolve these issues, we have developed a new method for the computation of *VT*-flash which is based on constrained minimization of the total Helmholtz free energy rather than equation solving. The minimization approach allows to solve all the issues mentioned above. As the method is based on the Newton–Raphson iterations, its convergence is fast compared to SSI. Unlike SSI, the new method guarantees that the total Helmholtz free energy of the system decreases in every iteration. Therefore, the method always converges to a state corresponding to a local minimum of A. As we use the results of stability to initialize the iteration, once the stability analysis decides that the system is in two-phase, convergence towards the false trivial solution is avoided.

The paper is structured as follows. In Section 2, we formulate the *VT*-flash problem and derive the equilibrium conditions using the Helmholtz free energy. In Section 3, we describe the new computational algorithm for calculation of phase-equilibria at constant volume, temperature, and moles. In Section 4, we describe construction of the initial guess using the results of *VT*-stability testing. In Section 5, we summarize the essential steps of the algorithm. In Section 6, we present numerical examples showing the performance of the algorithm on several mixtures of different degree of complexity. In Section 7, we discuss the results and draw some conclusions. In Appendix A, we summarize details of the equations of state that were used in the computations.

2. Conditions for phase equilibrium

Consider a mixture of n components with mole numbers $N_1, \ldots, N_n$ occupying volume V at temperature T. Let us assume the system is unstable and splits into two phases. We are interested in calculating volumes of both phases V' and V'', mole numbers of each component in both phases N_i' and N_i'' for $i = 1, \ldots, n$ and the pressure of the system P.

For single-phase systems, the Helmholtz free energy is given by

$$A^I = A(V, T, N_1, \ldots, N_n) = -PV + \sum_{i=1}^{n} N_i \mu_i, \tag{1}$$

where $P = P(V, T, N_1, \ldots, N_n)$ is the pressure given by a pressure-explicit equation of state, and $\mu_i = \mu_i(V, T, N_1, \ldots, N_n)$ is the chemical potential of the ith component in the mixture. For two-phase systems, the total Helmholtz free energy reads as

$$A^{II} = A(V', T, N_1', \ldots, N_n') + A(V'', T, N_1'', \ldots, N_n''). \tag{2}$$

The equilibrium state of the system is the one for which the total Helmholtz free energy increase with respect to the hypothetical single phase system,

$$\Delta A = A(V', T, N_1', \ldots, N_n') + A(V'', T, N_1'', \ldots, N_n'') - A(V, T, N_1, \ldots, N_n), \tag{3}$$

is minimal among all states satisfying the following $(n+1)$ constraints, which express the volume balance and mole balance

$$V' + V'' = V, \tag{4}$$

$$N_i' + N_i'' = N_i, \qquad i = 1, \ldots, n. \tag{5}$$

Using the Lagrange multiplier method, the system of $(n+1)$ necessary conditions of the phase equilibria is derived

$$P(V', T, N_1', \ldots, N_n') = P(V'', T, N_1'', \ldots, N_n''), \tag{6}$$

$$\mu_i(V', T, N_1', \ldots, N_n') = \mu_i(V'', T, N_1'', \ldots, N_n''), \qquad i = 1, \ldots, n. \tag{7}$$

These equations are the basis for equation solving methods like SSI developed in [9]. In this paper, we develop an optimization method, which is based on direct minimization of ΔA subject to the constraints (4) and (5). The same problem could also be formulated

using the minimization of A rather than ΔA. Obviously, the two formulations yield the same equilibrium states as the last term on the right hand side of (3) is constant. There are two advantages of using ΔA. First, while A can be evaluated up to an unknown additive constant, the expression for ΔA can be evaluated readily from the equation state. Second, ΔA is used in stability testing and the sign of ΔA shows whether a given two-phase split is more stable than the hypothetical single-phase state. This feature helps in the initialization of the algorithm (see Eq. (27) in Section 4).

3. Numerical algorithm for computation of phase equilibrium

We derive a numerical procedure for computing two-phase equilibrium at constant temperature, volume, and moles based on minimization of the total Helmholtz free energy of the two-phase system (3), which is subject to the volume and mole balance constraints (4) and (5).

The constraint equations (4) and (5) can be written in the matrix form with matrix $\mathbb{A} \in \mathrm{R}^{(n+1)\times(2n+2)}$, vector of unknowns $\mathbf{x} \in \mathrm{R}^{2n+2}$ and the vector of right hand side $\mathbf{b} \in \mathrm{R}^{n+1}$ as $\mathbb{A}\mathbf{x} = \mathbf{b}$, or

$$\underbrace{\begin{pmatrix} 1 & & & & 0 & 1 & & & & 0 \\ & 1 & & & 0 & & 1 & & & 0 \\ & & \ddots & & \vdots & & & \ddots & & \vdots \\ & & & 1 & 0 & & & & 1 & 0 \\ 0 & 0 & \dots & 0 & 1 & 0 & 0 & \dots & 0 & 1 \end{pmatrix}}_{\mathbb{A}} \underbrace{\begin{pmatrix} N_1' \\ \vdots \\ N_n' \\ V' \\ N_1'' \\ \vdots \\ N_n'' \\ V'' \end{pmatrix}}_{\mathbf{x}} = \underbrace{\begin{pmatrix} N_1 \\ N_2 \\ \vdots \\ N_n \\ V \end{pmatrix}}_{\mathbf{b}}. \tag{8}$$

As the matrix $\mathbb{A}$ has the full rank, the optimization problem with $2n+2$ unknowns and $n+1$ linearly independent linear constraints can be transformed into an unconstrained problem in $2n+2-(n+1) = n+1$ variables. In principle, one could use the constraints to eliminate one set of unknowns (say V'', and $N_1'', \dots, N_n''$) and formulate the problem as an unconstrained optimization problem in the other set of variables (V', and $N_1', \dots, N_n'$). This would lead to a non-symmetric formulation preffering one phase over the other one. This may cause some problems in numerical computation if, for example, one of the phases in the two-phase system occurs in a very small amount. In our method we use a different approach based on the LQ-factorization of matrix $\mathbb{A}$, which can treat all phases in a unified way. The symmetry of our formulation is an advantageous feature that makes the method robust even in these limit situations. The reduction in dimensionality can be performed using two subspaces $\mathcal{Y}$ and $\mathcal{Z}$, where $\mathcal{Y}$ is the $(n+1)$-dimensional subspace of R^{2n+2} spanned by the rows of matrix $\mathbb{A}$ and $\mathcal{Z}$ is $(n+1)$-dimensional subspace of R^{2n+2} of vectors orthogonal to the rows of matrix $\mathbb{A}$. As

$$\mathrm{R}^{2n+2} = \mathcal{Y} \oplus \mathcal{Z}, \tag{9}$$

any $(2n+2)$-dimensional vector $\mathbf{x}$ can be uniquely written as a sum of vectors from $\mathcal{Y}$ and $\mathcal{Z}$ as

$$\mathbf{x} = \mathbb{Y}\mathbf{x}_{\mathcal{Y}} + \mathbb{Z}\mathbf{x}_{\mathcal{Z}}, \tag{10}$$

where $\mathbb{Y}$ and $\mathbb{Z}$ denote matrices from $\mathrm{R}^{(2n+2)\times(n+1)}$ whose columns represent bases of subspaces $\mathcal{Y}$ and $\mathcal{Z}$, respectively, the $(n+1)$-dimensional vector $\mathbf{x}_{\mathcal{Y}}$ is called the range-space part of $\mathbf{x}$, and the $(n+1)$-dimensional vector $\mathbf{x}_{\mathcal{Z}}$ is called the null-space part of $\mathbf{x}$. The solution $\mathbf{x}^*$ of the constrained optimization problem, given by $\mathrm{x}^* = \mathrm{Y}\mathbf{x}_{\mathrm{Y}}^* + \mathrm{Z}\mathbf{x}_{\mathrm{Z}}^*$, is feasible, therefore

$$\mathbb{A}\mathbf{x}^* = \mathbb{A}(\mathbb{Y}\mathbf{x}_{\mathcal{Y}}^* + \mathbb{Z}\mathbf{x}_{\mathcal{Z}}^*) = \mathbf{b}.$$

From the definition of the subspace $\mathcal{Z}$, it follows that $\mathbb{A}\mathbb{Z} = 0$, and

$$\mathbb{A}\mathbb{Y}\mathbf{x}_{\mathcal{Y}}^* = \mathbf{b}.$$

From the definition of subspace $\mathcal{Y}$ it follows that the matrix $\mathbb{A}\mathbb{Y}$ is non-singular, so the vector $\mathbf{x}_{\mathcal{Y}}^*$ is uniquely determined by the previous equation. Similarly, any feasible vector $\mathbf{x}$ must have the same range-space part, that means $\mathbf{x}_{\mathcal{Y}} = \mathbf{x}_{\mathcal{Y}}^*$, and on the contrary, any vector with range-space component $\mathbf{x}_{\mathcal{Y}}^*$ satisfies the constraints of the optimization problem. So the range-space part $\mathbf{x}_{\mathcal{Y}}^*$ of the solution is uniquely determined by the constraints, and only the $(n+1)$-dimensional part $\mathbf{x}_{\mathcal{Z}}^*$ remains unknown.

To represent the null-space $\mathcal{Z}$, we use the LQ-factorization of matrix $\mathbb{A}$ [12]. Let $\mathbb{Q} \in \mathrm{R}^{(2n+2)\times(2n+2)}$ be an orthogonal matrix such that

$$\mathbb{A}\mathbb{Q} = (\mathbb{L} \quad 0), \tag{11}$$

where $\mathbb{L} \in \mathrm{R}^{(n+1)\times(n+1)}$ is a non-singular lower triangular matrix. From this it can be seen that the matrix $\mathbb{Y}$ can be chosen as the first $n+1$ columns of matrix $\mathbb{Q}$ and the matrix $\mathbb{Z}$ can be chosen as the remaining $n+1$ columns of $\mathbb{Q}$, i.e.

$$\mathbb{Q} = (\mathbb{Y} \quad \mathbb{Z}). \tag{12}$$

If we denote the identity matrix in R^{n+1} as $\mathbb{I}_{n+1}$, the matrix $\mathbb{A}$ can be written as $\mathbb{A} = (\mathbb{I}_{n+1} \quad \mathbb{I}_{n+1})$. The matrices $\mathbb{Y}$ and $\mathbb{Z}$ then read as

$$\mathbb{Y} = \frac{1}{\sqrt{2}}\mathbb{A}^T = \frac{1}{\sqrt{2}}\begin{pmatrix} \mathbb{I}_{n+1} \\ \mathbb{I}_{n+1} \end{pmatrix}, \quad \mathbb{Z} = \frac{1}{\sqrt{2}}\begin{pmatrix} \mathbb{I}_{n+1} \\ -\mathbb{I}_{n+1} \end{pmatrix}. \tag{13}$$

Our algorithm for solving the optimization problem is iterative. Provided that we start from a feasible initial guess $\mathbf{x}^{(0)}$, the algorithm generates a sequence of feasible iterates $\mathbf{x}^{(k)}$. In every iteration, $\mathbf{x}^{(k)}$ is updated as

$$\mathbf{x}^{(k+1)} = \mathbf{x}^{(k)} + \alpha_k \mathbf{d}^{(k)},$$

where $\alpha_k > 0$ denotes the step size and $\mathbf{d}^{(k)}$ denotes the direction vector. Assuming that $\mathbf{x}^{(k)}$ is feasible, we require that $\mathbf{x}^{(k+1)}$ be feasible too. To satisfy this, it is necessary that the direction vector $\mathbf{d}^{(k)}$ be orthogonal to the rows of $\mathbb{A}$, i.e.

$$\mathbb{A}\mathbf{d}^{(k)} = 0, \tag{14}$$

or equivalently

$$\mathbf{d}^{(k)} = \mathbb{Z}\mathbf{d}_{\mathcal{Z}}^{(k)}, \tag{15}$$

for a suitable $(n+1)$-dimensional vector $\mathbf{d}_{\mathcal{Z}}^{(k)}$. It is obvious that the search direction $\mathbf{d}^{(k)}$ is a $(2n+2)$-dimensional vector, which is constructed to lie in a $(n+1)$-dimensional subspace $\mathcal{Z}$. The columns of matrix $\mathbb{Z}$ forming an orthogonal basis of $\mathcal{Z}$ are given by (13), so it remains to determine the vector $\mathbf{d}_{\mathcal{Z}}^{(k)} \in \mathrm{R}^{n+1}$. This way we have transformed the constrained minimization problem to an unconstrained problem in a lower dimension.

To find the vector $\mathbf{d}_{\mathcal{Z}}^{(k)}$, we use the modified Newton method, which is based on the quadratic approximation of function ΔA around the point $\mathbf{x}^{(k)}$. Let us denote by $\mathbf{g}(\mathbf{x})$ the gradient of the

function ΔA. By partial differentiating of ΔA with respect to its variables, we obtain

$$\mathbf{g}(\mathbf{x}) = \nabla(\Delta A)^T = \begin{pmatrix} \mu_1(V', T, N_1', \dots, N_n') \\ \vdots \\ \mu_n(V', T, N_1', \dots, N_n') \\ -P(V', T, N_1', \dots, N_n') \\ \mu_1(V'', T, N_1'', \dots, N_n'') \\ \vdots \\ \mu_n(V'', T, N_1'', \dots, N_n'') \\ -P(V'', T, N_1'', \dots, N_n'') \end{pmatrix}. \tag{16}$$

Next, let us denote by $\mathbb{H}(\mathbf{x})$ the Hessian of the function ΔA obtained in the following block-diagonal form

$$\mathbb{H}(\mathbf{x}) = \nabla^2 \Delta A = \begin{pmatrix} \mathbb{B}' & \mathbb{C}' & & \\ \mathbb{C}'^T & \mathbb{D}' & & \\ & & \mathbb{B}'' & \mathbb{C}'' \\ & & \mathbb{C}''^T & \mathbb{D}'' \end{pmatrix}, \tag{17}$$

where

$$\begin{aligned}
&\mathbb{B}' \in \mathrm{R}^{n\times n}, \quad \mathbb{B}'_{ij} = \frac{\partial \mu_i}{\partial N_j'}(V', T, N_1', \dots, N_n'), \\
&\mathbb{B}'' \in \mathrm{R}^{n\times n}, \quad \mathbb{B}''_{ij} = \frac{\partial \mu_i}{\partial N_j''}(V'', T, N_1'', \dots, N_n''), \\
&\mathbb{C}' \in \mathrm{R}^{n}, \quad \mathbb{C}'_{j} = -\frac{\partial P}{\partial N_j'}(V', T, N_1', \dots, N_n'), \\
&\mathbb{C}'' \in \mathrm{R}^{n}, \quad \mathbb{C}''_{j} = -\frac{\partial P}{\partial N_j''}(V'', T, N_1'', \dots, N_n''), \\
&\mathbb{D}' \in \mathrm{R}^{1}, \quad \mathbb{D}' = -\frac{\partial P}{\partial V'}(V', T, N_1', \dots, N_n'), \\
&\mathbb{D}'' \in \mathrm{R}^{1}, \quad \mathbb{D}'' = -\frac{\partial P}{\partial V''}(V'', T, N_1'', \dots, N_n'')
\end{aligned}.$$

Approximating the function ΔA using the Taylor expansion around the point $\mathbf{x}^{(k)}$ up to the quadratic terms, the search direction $\mathbf{d}^{(k)} = \mathbb{Z}\mathbf{d}_{\mathcal{Z}}^{(k)}$ is found as a solution of the following minimization problem

$$\begin{aligned}
&\min_{\substack{\mathbf{d}^{(k)}\in \mathrm{R}^{(2n+2)} \\ \mathbb{A}\mathbf{d}^{(k)} = 0}} \Delta A(\mathbf{x}^{(k)} + \mathbf{d}^{(k)}) = \min_{\mathbf{d}_{\mathcal{Z}}^{(k)}\in \mathrm{R}^{(n+1)}} \Delta A(\mathbf{x}^{(k)} + \mathbb{Z}\mathbf{d}_{\mathcal{Z}}^{(k)}) \\
&\approx \min_{\mathbf{d}_{\mathcal{Z}}^{(k)}\in \mathrm{R}^{(n+1)}} \Delta A(\mathbf{x}^{(k)}) + \mathbf{g}(\mathbf{x}^{(k)})^T \mathbb{Z}\mathbf{d}_{\mathcal{Z}}^{(k)} + \frac{1}{2}(\mathbb{Z}\mathbf{d}_{\mathcal{Z}}^{(k)})^T \mathbb{H}(\mathbf{x}^{(k)})\mathbb{Z}\mathbf{d}_{\mathcal{Z}}^{(k)}.
\end{aligned} \tag{18}$$

The vector $\mathbf{d}_{\mathcal{Z}}^{(k)}$ is the argument of minimum of a quadratic function Φ defined as

$$\Phi(\mathbf{d}_{\mathcal{Z}}) = \mathbf{g}(\mathbf{x}^{(k)})^T \mathbb{Z}\mathbf{d}_{\mathcal{Z}} + \frac{1}{2}\mathbf{d}_{\mathcal{Z}}^T \mathbb{Z}^T \mathbb{H}(\mathbf{x}^{(k)})\mathbb{Z}\mathbf{d}_{\mathcal{Z}}.$$

The function Φ has a stationary point if and only if there is a $\mathbf{d}_{\mathcal{Z}}^{(k)}$, for which the gradient of Φ vanishes, i.e.

$$\nabla\Phi(\mathbf{d}_{\mathcal{Z}}^{(k)}) = 0. \tag{19}$$

The stationary point $\mathbf{d}_{\mathcal{Z}}^{(k)}$ is a solution of the following system of equations

$$\mathbb{H}_{\mathcal{Z}}(\mathbf{x}^{(k)})\mathbf{d}_{\mathcal{Z}}^{(k)} = -\mathbf{g}_{\mathcal{Z}}(\mathbf{x}^{(k)}), \tag{20}$$

where $\mathbb{H}_{\mathcal{Z}}(\mathbf{x}^{(k)}) \in \mathrm{R}^{(n+1)\times(n+1)}$ and $\mathbf{g}_{\mathcal{Z}}(\mathbf{x}^{(k)}) \in \mathrm{R}^{n+1}$ are the restrictions of the Hessian and of the gradient vector to the subspace $\mathcal{Z}$ defined as

$$\mathbb{H}_{\mathcal{Z}}(\mathbf{x}^{(k)}) = \mathbb{Z}^T \mathbb{H}(\mathbf{x}^{(k)})\mathbb{Z} \tag{21}$$

and

$$\mathbf{g}_{\mathcal{Z}}(\mathbf{x}^{(k)}) = \mathbb{Z}^T \mathbf{g}(\mathbf{x}^{(k)}). \tag{22}$$

Combining (13), (16), and (17), it follows from (21) and (22) that

$$\mathbb{H}_{\mathcal{Z}}(\mathbf{x}^{(k)}) = \frac{1}{2}\begin{pmatrix} \mathbb{B} & \mathbb{C} \\ \mathbb{C}^T & \mathbb{D} \end{pmatrix}, \tag{23}$$

where

$$\begin{aligned}
&\mathbb{B} \in \mathrm{R}^{n\times n}, \mathbb{B}_{ij} = \frac{\partial \mu_i}{\partial N_j'}(V', T, N_1', \dots, N_n') + \frac{\partial \mu_i}{\partial N_j''}(V'', T, N_1'', \dots, N_n''), \\
&\mathbb{C} \in \mathrm{R}^{n}, \mathbb{C}_j = -\frac{\partial P}{\partial N_j'}(V', T, N_1', \dots, N_n') - \frac{\partial P}{\partial N_j''}(V'', T, N_1'', \dots, N_n'') \\
&\mathbb{D} \in \mathrm{R}^{1}, \mathbb{D} = -\frac{\partial P}{\partial V'}(V', T, N_1', \dots, N_n') - \frac{\partial P}{\partial V''}(V'', T, N_1'', \dots, N_n''),
\end{aligned}$$

and

$$\mathbf{g}_{\mathcal{Z}}(\mathbf{x}^{(k)}) = \frac{1}{\sqrt{2}}\begin{pmatrix} \mu_1(V', T, N_1', \dots, N_n') - \mu_1(V'', T, N_1'', \dots, N_n'') \\ \vdots \\ \mu_n(V', T, N_1', \dots, N_n') - \mu_n(V'', T, N_1'', \dots, N_n'') \\ -P(V', T, N_1', \dots, N_n') + P(V'', T, N_1'', \dots, N_n'') \end{pmatrix}. \tag{24}$$

Note that the gradient vector in (16) depends on the values of chemical potentials, which are determined up to an arbitrary constant. Unlike in (16), the restricted gradient given by (24) is a function of differences of the chemical potentials between two states whose values can be evaluated uniquely using the equation of state [9]. Unlike in [7], our formulation does not require to use the complex arithmetics.

If $\mathbf{d}_{\mathcal{Z}}^{(k)}$ solves the system of the equations (20) and the matrix $\mathbb{H}_{\mathcal{Z}}$ is positive definite, then the search direction $\mathbf{d}_{\mathcal{Z}}^{(k)}$ is a descent direction. If the matrix of the projected Hessian is not positive definite, then either the quadratic approximation of the function is not bounded from below, or a single minimum does not exist. In this

case, it is necessary to modify the direction $\mathbf{d}_{\mathcal{Z}}^{(k)}$. If the matrix $\mathbb{H}_{\mathcal{Z}}$ is indefinite, then the vector $\mathbf{d}_{\mathcal{Z}}^{(k)}$ is found as a solution of a modified system of the equations

$$\widehat{\mathbb{H}_{\mathcal{Z}}}(\mathbf{x}^{(k)})\mathbf{d}_{\mathcal{Z}}^{(k)} = -\mathbf{g}_{\mathcal{Z}}(\mathbf{x}^{(k)}), \tag{25}$$

where $\widehat{\mathbb{H}_{\mathcal{Z}}}(\mathbf{x}^{(k)})$ is a positive definite matrix obtained by the modified Cholesky decomposition of the matrix $\mathbb{H}_{\mathcal{Z}}(\mathbf{x}^{(k)})$. In this algorithm the usual Cholesky factorization is performed to decompose matrix $\mathbb{H}_{\mathcal{Z}}(\mathbf{x}^{(k)})$ into the product $\mathbb{L}\mathbb{L}^T$ where $\mathbb{L}$ is a lower triangular matrix. If a negative element appears on the diagonal of $\mathbb{L}$ during the Cholesky factorization, a suitable value is added to this element to ensure its positivity in the final decomposition. This way we obtain the Cholesky factorization of a positive definite matrix $\widehat{\mathbb{H}_{\mathcal{Z}}}(\mathbf{x}^{(k)})$, which is used instead of matrix $\mathbb{H}_{\mathcal{Z}}(\mathbf{x}^{(k)})$ in (25) to determine the direction $\mathbf{d}_{\mathcal{Z}}^{(k)}$ in the Newton method. This modification of the Newton method ensures that the obtained direction is a descent direction. Therefore, for a sufficiently small step size $\alpha_k > 0$, the decrease of ΔA can be guaranteed. The following line-search technique can be used to find the step size α_k. First, we put $\alpha_k = 1$ and test if $\Delta A(\mathbf{x}^{(k)} + \mathbf{d}^{(k)}) < \Delta A(\mathbf{x}^{(k)})$. If this condition is satisfied, we set $\mathbf{x}^{(k+1)} = \mathbf{x}^{(k)} + \mathbf{d}^{(k)}$. If the condition is violated, we halve the value of α_k until the condition $\Delta A(\mathbf{x}^{(k)} + \alpha_k\mathbf{d}^{(k)}) < \Delta A(\mathbf{x}^{(k)})$ is satisfied and then set $\mathbf{x}^{(k+1)} = \mathbf{x}^{(k)} + \alpha_k\mathbf{d}^{(k)}$. This completes a single iteration of the Newton method. The iterations are terminated when a suitable stopping criterion is satisfied or the method continues with the next iteration if needed. In this work, we stop the iterations if (cf. [13])

$$\|\mathbf{d}^{(k)}\|_2 := \left(\sum_{j=1}^{2n+2} \mathbf{d}_j^{(k)2}\right)^{1/2} \leq \varepsilon_{tol} = 10^{-7}. \tag{26}$$

4. Initialization of the *VT*-flash algorithm

To initialize the algorithm, an initial guess $\mathbf{x}^{(0)}$ is needed. We use the *VT*-stability test from [10] before the *VT*-flash calculation to test whether the single phase is stable or not at given volume V, temperature T, and mole numbers $N_1, \ldots, N_n$. Denoting by $c_i = N_i/V$ the overall molar concentrations of all components, the *VT*-stability algorithm tests whether a trial phase with concentrations c_i' can be found such that, if taken in a small amount from the initial phase, the two-phase system will have lower total Helmholtz free energy than the single-phase system. From this, the following criterion of stability at constant volume, temperature, and moles can be derived (see [10] for details). The single phase is stable if

$$\begin{aligned} &D(T, c_1', \ldots, c_n') \\ &\quad = \lim_{V' \to 0+} \frac{\Delta A}{V'} = \sum_{i=1}^{n} [\mu_i(1, T, c_1', \ldots, c_n') - \mu_i(1, T, c_1, \ldots, c_n)]c_i' \\ &\qquad -[P(1, T, c_1', \ldots, c_n') - P(1, T, c_1, \ldots, c_n)] \geq 0 \end{aligned} \tag{27}$$

for all admissible states $(T, c_1', \ldots, c_n')$. If this condition is satisfied, the system is in single-phase and the *VT*-flash calculation is avoided (pressure can be computed using the equation of state). In the opposite case, the mixture splits into phases and the *VT*-stability algorithm provides trial phase concentrations c_i' such that $D(T, c_1', \ldots, c_n') < 0$. As $D(T, c_1', \ldots, c_n') = \lim_{V' \to 0+} \Delta A/V' < 0$, we can use the bisection method to find a small volume $V' > 0$ such that $\Delta A < 0$ for a state in which one phase is the trial phase with volume V' and mole numbers $N_i' = c_i'V'$ and the other phase properties V'' and N_i'' are computed such that (4) and (5) hold. This way we construct a two-phase state with lower total Helmholtz free energy than the initial single-phase state. As the *VT*-flash algorithm guarantees to decrease the total Helmholtz free energy in every iteration, the possibility of convergence toward the trivial solution is excluded.

5. Algorithm of the modified Newton method for *VT*-flash

Now, we are ready to summarize the essential steps of our algorithm.

Step 1 Let $N_1, \ldots, N_n$, V and $T > 0$ be given. Set the number of iterations $k = 0$. Get an initial feasible solution $\mathbf{x}^{(0)} \in \mathrm{R}^{2n+2}$ from the *VT*-stability algorithm

$$\mathbf{x}^{(0)} = \begin{pmatrix} N_1' \\ \vdots \\ N_n' \\ V' \\ N_1'' \\ \vdots \\ N_n'' \\ V'' \end{pmatrix}. \tag{28}$$

Step 2 Assemble the Hessian $\mathbb{H}_{\mathcal{Z}}(\mathbf{x}^{(k)})$ and the gradient $\mathbf{g}_{\mathcal{Z}}(\mathbf{x}^{(k)})$ of ΔA in the kth iteration projected to the subspace $\mathcal{Z}$ using (23) and (24).

Step 3 Compute the projected step direction $\mathbf{d}_{\mathcal{Z}}^{(k)} \in \mathrm{R}^{n+1}$, and the feasible direction $\mathbf{d}^{(k)} \in \mathrm{R}^{2n+2}$ by

$$\mathbb{H}_{\mathcal{Z}}(\mathbf{x}^{(k)})\mathbf{d}_{\mathcal{Z}}^{(k)} = -\mathbf{g}_{\mathcal{Z}}(\mathbf{x}^{(k)}), \tag{29}$$

$$\mathbf{d}^{(k)} = \mathbb{Z}\mathbf{d}_{\mathcal{Z}}^{(k)}. \tag{30}$$

If the matrix $\mathbb{H}_{\mathcal{Z}}(\mathbf{x}^{(k)})$ is not positive definite, find the vector $\mathbf{d}_{\mathcal{Z}}^{(k)}$ by solving a modified system of equations

$$\widehat{\mathbb{H}_{\mathcal{Z}}}(\mathbf{x}^{(k)})\mathbf{d}_{\mathcal{Z}}^{(k)} = -\mathbf{g}_{\mathcal{Z}}(\mathbf{x}^{(k)}), \tag{31}$$

where $\widehat{\mathbb{H}_{\mathcal{Z}}}(\mathbf{x}^{(k)})$ is a positive definite matrix obtained from the modified Cholesky factorization of matrix $\mathbb{H}_{\mathcal{Z}}(\mathbf{x}^{(k)})$.

Step 4 Determine the step length $\alpha_k > 0$ for the kth iteration satisfying

$$\Delta A(\mathbf{x}^{(k)} + \alpha_k\mathbf{d}^{(k)}) < \Delta A(\mathbf{x}^{(k)}). \tag{32}$$

First, set the step length to $\alpha_k = 1$ and test if the condition (32) holds. If not, use the bisection method to find a value of α_k satisfying (32).

Step 5 Update the approximation as

$$\mathbf{x}^{(k+1)} = \mathbf{x}^{(k)} + \alpha_k\mathbf{d}^{(k)}. \tag{33}$$

Step 6 Test the convergence using (26). If needed, increase k by 1 and go to Step 2. If not needed, the algorithm ends up with the solution $\mathbf{x}^{(k+1)}$.

6. Numerical examples of *VT*-flash calculations

We have tested the algorithm in several examples for binary and multi-component mixtures under different conditions. First, we have tested the *VT*-flash algorithm on all examples of mixtures from [9]. The new algorithm converged well in all cases and provided the same solutions as those reported in [9]. In all cases the

Table 1
Numbers of iterations for the VT-flash algorithm developed in this paper and the succesive substitution iteration (SSI) from [9] for five mixtures investigated in [9]. Example numbers refer to Examples in [9]. The detailed description of the mixtures and conditions can be found in [9].

Number of iterations	VT-flash (this work)	VT-flash SSI [9]
Example 1	6	46
Example 2	6	20
Example 3	6	25
Example 4 (with N_2)	6	33
Example 4 (with CO_2)	6	266

Table 2
Parameters of the Peng–Robinson and CPA equations of state for all components used in all examples.

Component	$T_{i,crit}$ [K]	$P_{i,crit}$ [MPa]	ω_i	$M_{w,i}$ [kg kmol^{-1}]
H_2O	647.29	22.09	0.3440	18.01528
CO_2	304.14	7.375	0.2390	44.0
N_2	126.21	3.390	0.0390	28.0
C_1	190.56	4.599	0.0110	16.0
C_3	369.83	4.248	0.1530	44.1
nC_5	469.70	3.370	0.2510	72.2
C_6	507.40	3.012	0.2960	86.2
nC_{10}	617.70	2.110	0.4890	142.28

new method needed much less iterations than the SSI method from [9]. The numbers of iterations for both methods are summarized in Table 1.

In the following examples, we simulate isothermal compression of a mixture in a closed cell. The *VT*-stability algorithm from [10] is used to detect the boundary between the stable single-phase and two-phase regions for an interval of temperatures and for the whole range of admissible molar concentrations c. For a selected temperature T, we change the overall molar concentration c and provide results of the *VT*-flash calculations for the mixture at temperature T and molar concentrations $c_i = cz_i$. We present six examples of different complexity. In Examples 1–5, we use the Peng–Robinson equastion of state. Parameters of the Peng–Robinson equation of state for all components used are presented in Table 2. For Example 6, we use the Cubic-Plus-Association (CPA) equation of state. Details for both the equations of state can be found in Appendix A.

Note that in the following examples *VT*-flash algorithm is used to evaluate amount and properties of the split phases, generally denoted as phase 1 and phase 2. We have not attempted to perform any phase identification or post processing of the results. Therefore, the numbering of the phases depends solely on the result of the minimization procedure. In some figures we can observe swapping of the two-phases at certain points but this effect has no physical significance.

Example 1

In the first example, we investigate two-phase equilibrium for pure carbon dioxide (CO_2). The approximate boundary between the single-phase and two-phase domains in the c, T-space obtained from *VT*-stability analysis is shown in Fig. 1 (left). As shown in Fig. 1 (left), at temperature $T = 280$ K the mixture occurs in single-phase for low enough molar densities. During isothermal compression, at moderate molar concentrations the mixture splits into two phases, while at high molar densities (higher than 20 kmol m^{-3}) the mixture becomes single-phase again. We show the saturations (volume fractions) of both phases and mass densities of both phases as functions of the overall molar density c in Fig. 2. The equilibrium pressure for each overall molar concentration c is presented in Fig. 1 (right).

Note that within the two-phase region (between points A and B in Fig. 1 (right)), the pressure is constant and equal to the saturation pressure P_{sat} corresponding to the temperature $T = 280$ K. All these states occur at the same pressure P, temperature T, and mole number N. Therefore, *PT*-stability and *PT*-flash cannot distinguish between these states. As these states have different volumes, the *VT*-based formulation can distinguish between them. This example shows that the variables P, T, N are not equivalent to V, T, N in the sense that specifying the volume, temperature and moles uniquely determines the equilibrium state of the system. This is not the case of the P, T, N formulation in which all two-phase states and both saturated gas (point A in Fig. 1 (right)) and saturated liquid (point B in Fig. 1 (right)) occur at the same values of P, T, N.

There are also other advantages of the volume-based formulations. Consider applying *PT*-stability and *PT*-flash to a pure component system at temperature T and pressures $P_1 = P_{sat}(T) + \varepsilon$ and $P_2 = P_{sat}(T) - \varepsilon$, where $\varepsilon > 0$ is an arbitrarily small number. For both cases, the system is in single-phase. For P_1 we have an almost saturated liquid with molar concentration c_1, for P_2 we have an almost saturated gas with molar concentration $c_2 < c_1$. While the difference of pressures $P_1 - P_2$ is very small, the difference in concentrations $c_1 - c_2$ may be large, i.e. although the pressure change is small, the volume of the system changes a lot. The discontinuous jump in volume associated with a small change in pressure may

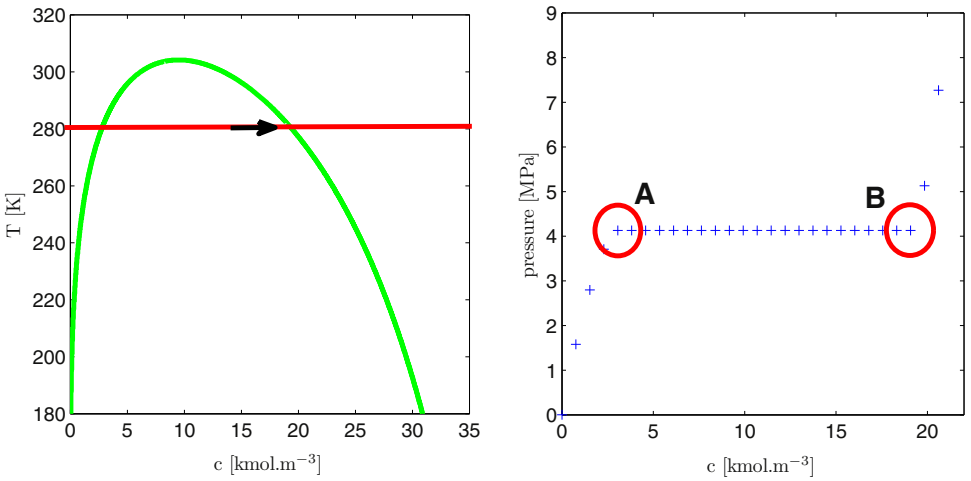

Fig. 1. Approximate boundary between the single-phase and two-phase domains in the c, T-space (left). The arrow indicates the compression at constant temperature $T = 280$ K. Equilibrium pressure as a function of the overall molar density c at $T = 280$ K (right). Example 1: pure CO_2.

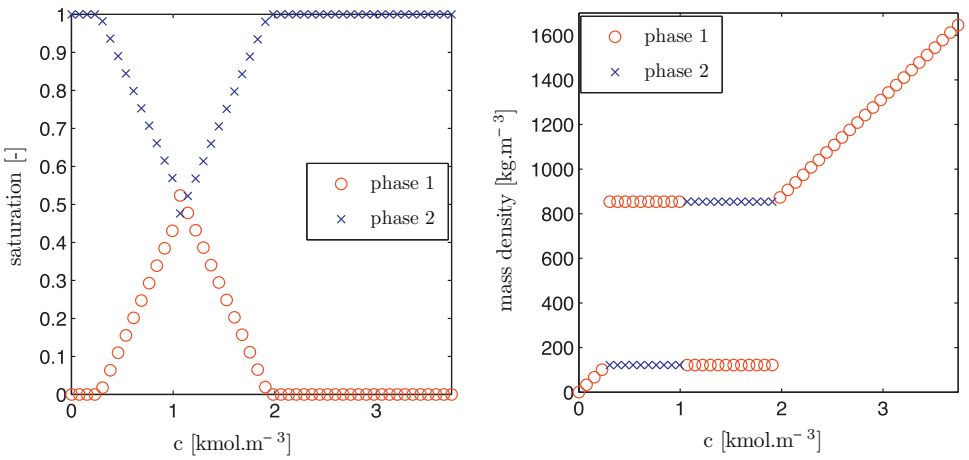

Fig. 2. Saturations (left) and mass densities (right) of both phases as functions of the overall molar density c. Example 1: pure CO_2 at $T = 280$ K.

cause convergence problems in numerical methods applied to the solution of the *PT*-flash. On the other hand, in the *VT*-formulation, the equilibrium pressure is a continuous function of the total volume of the system (cf. Fig. 1 (right)).

Example 2

In the second example, we investigate two-phase equilibrium for a binary mixture of methane (C_1) and normal pentane (nC_5) with mole fractions $z_{C_1} = 0.547413$ and $z_{nC_5} = 0.452587$. The binary interaction coefficient $\delta_{C_1-nC_5} = 0.041$. The approximate boundary between the single-phase and two-phase domains in the c, T-space obtained from *VT*-stability analysis is shown in Fig. 3 (left). As shown in Fig. 3 (left), at temperature $T = 371$ K the mixture occurs in single-phase for low molar densities. During isothermal compression, the mixture splits into two phases at moderate molar densities, while at high molar densities (higher than 9 kmol m^{-3}) the mixture becomes single-phase again.

The equilibrium pressure as a function of the overall molar density c is presented in Fig. 3 (right) illustrating a steady rise of the equilibrium pressure during compression, and its substantial increase at molar densities 9 kmol m^{-3} and higher when all gas is depleted. Saturations of both phases and mass densities of both phases as functions of the overall molar density c are presented in Fig. 4. Mole fractions of both components in both phases for each overall molar density c are presented in Fig. 5.

Example 3

In the third example, we investigate two-phase equilibrium for a binary mixture of carbon dioxide (CO_2) and normal decane (nC_{10}) with mole fractions $z_{CO_2} = 0.547413$ and $z_{C_{10}} = 0.452587$. The binary interaction coefficient $\delta_{CO_2-nC_{10}} = 0.150$. The approximate boundary between the single-phase and two-phase domains in the c, T-space obtained from *VT*-stability analysis is shown in Fig. 6 (left). As shown in Fig. 6, when compressing at constant temperature $T = 311$ K, the mixture occurs in two-phase from the lowest molar densities up to approximately 8 kmol m^{-3}, then the mixture becomes single-phase, while at molar densities higher than 9.5 kmol m^{-3} the mixture becomes two-phase again.

The equilibrium pressure as a function of the overall molar density c is presented in Fig. 6 (right) illustrating a steady rise of the equilibrium pressure during compression, and its substantial increase at molar densities 8 kmol m^{-3} and higher when all gas phase is depleted. Saturations of both phases and mass densities of both phases as functions of the overall molar density c are presented in Fig. 7. Mole fractions of both components in both

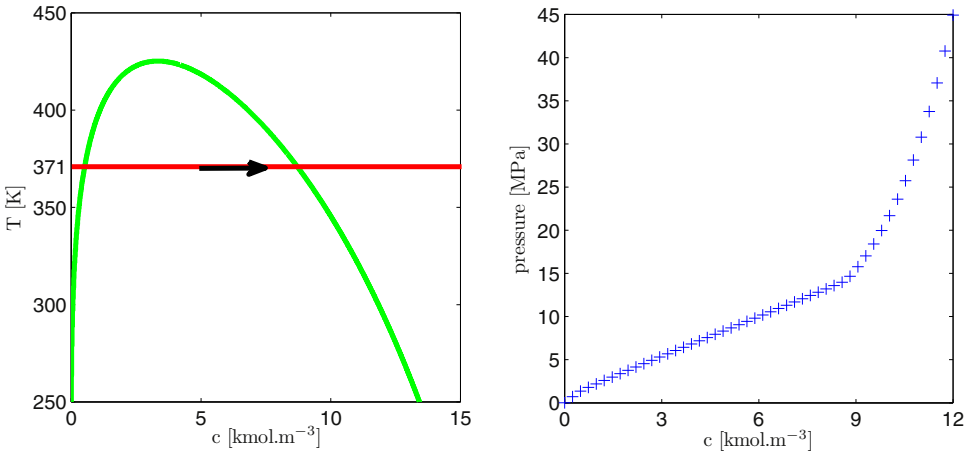

Fig. 3. Approximate boundary between the single-phase and two-phase domains in the c, T-space (left). The arrow indicates the compression at constant temperature $T = 371$ K. Equilibrium pressure as a function of the overall molar density c at $T = 371$ K (right). Example 2: binary C_1–nC_5 mixture ($z_{C_1} = 0.547413$, $z_{nC_5} = 0.452587$).

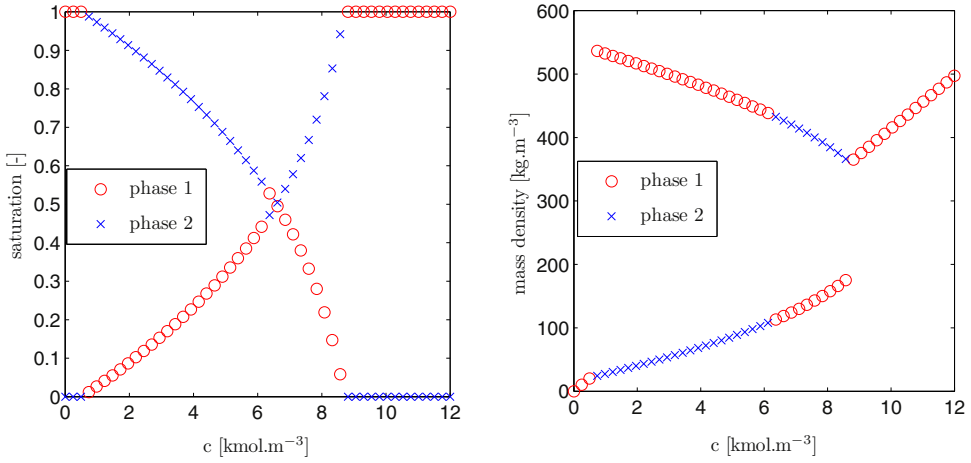

Fig. 4. Saturations (left) and mass densities (right) of both phases as functions of the overall molar density c. Example 2: binary C_1–nC_5 mixture ($z_{C_1} = 0.547413$, $z_{nC_5} = 0.452587$, and $T = 371$ K).

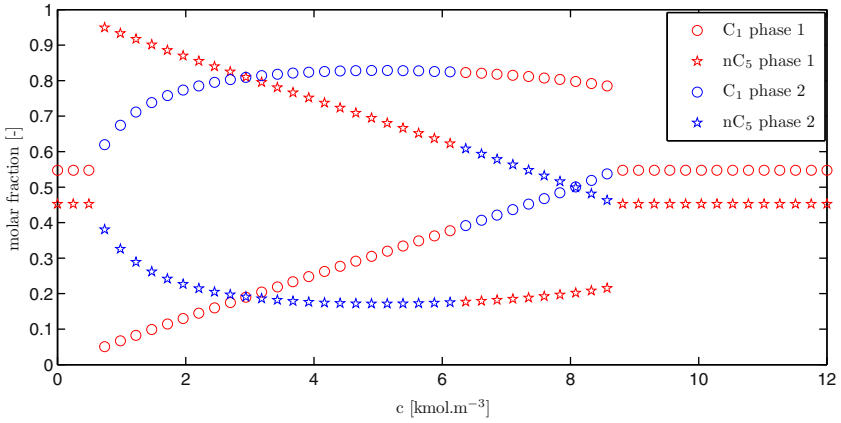

Fig. 5. Molar fractions of both components in both phases as functions of the overall molar density c at $T = 371$ K. Example 2: binary C_1–nC_5 mixture ($z_{C_1} = 0.547413$, $z_{nC_5} = 0.452587$).

phases as functions of the overall molar density c are presented in Fig. 8.

Figs. 6 (left) and 7 (right) suggest that the second two-phase region at high molar densities and low temperatures may correspond to a liquid–liquid two-phase region.

Example 4

In the fourth example, we investigate two-phase equilibrium for a ternary mixture of methane (C_1), hexane (C_6) and normal decane (nC_{10}) with mole fractions $z_{C_1} = 0.405946$, $z_{C_6} = 0.297027$ and

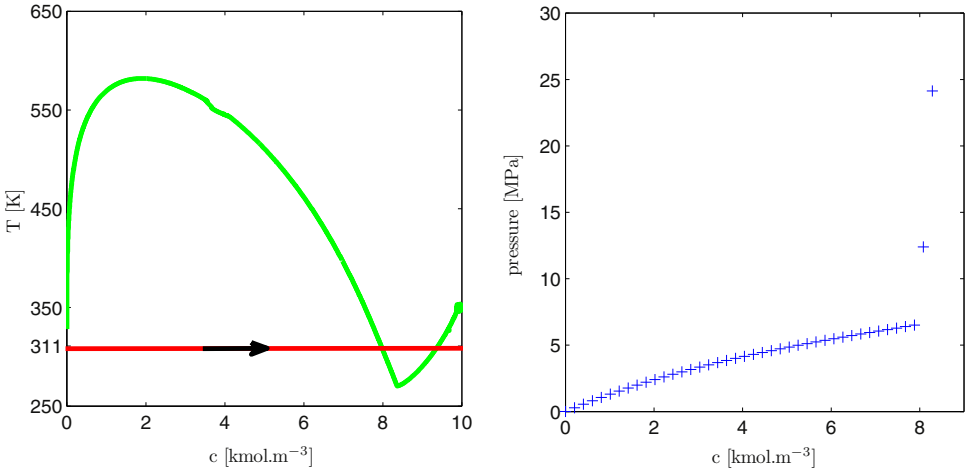

Fig. 6. Approximate boundary between the single-phase and two-phase domains in the c, T-space (left). The arrow indicates the compression at constant temperature $T = 311$ K. Equilibrium pressure as a function of the overall molar density c (right) at $T = 311$ K. Example 3: binary CO_2–nC_{10} mixture ($z_{CO_2} = 0.547413$, $z_{C_{10}} = 0.452587$).

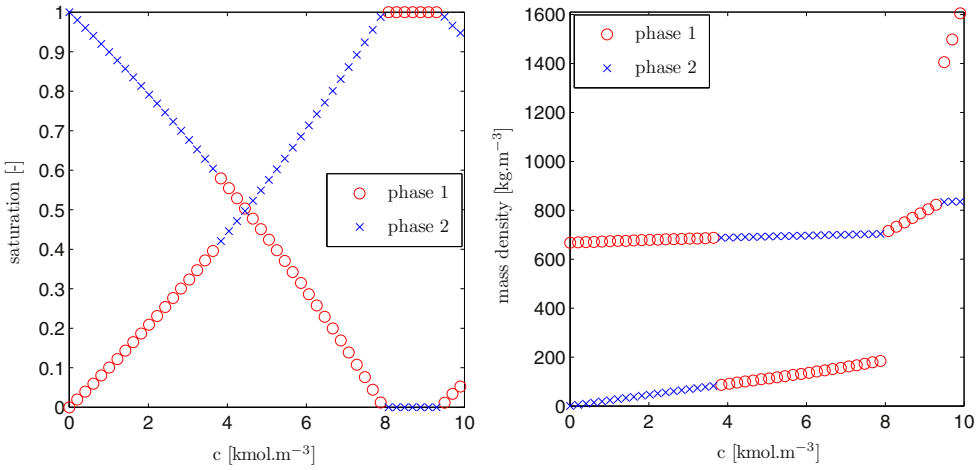

Fig. 7. Saturations (left) and mass densities of both phases as function of the overall molar density c (right). Example 3: binary CO_2–nC_{10} mixture ($z_{CO_2} = 0.547413$, $z_{C_{10}} = 0.452587$, and $T = 311$ K).

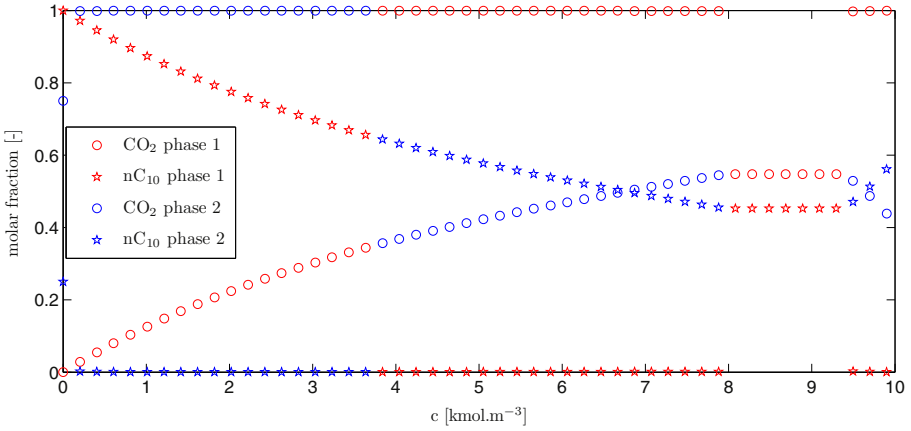

Fig. 8. Molar fractions of both components in both phases as functions of the overall molar density c at $T = 311$ K. Example 3: binary CO_2–nC_{10} mixture ($z_{CO_2} = 0.547413$, $z_{C_{10}} = 0.452587$).

$z_{C_{10}} = 0.297027$. The binary interaction coefficients are presented in Table 3. The approximate boundary between the single-phase and two-phase domains in the c, T-space obtained from VT-stability analysis is shown in Fig. 9 (left). As shown in Fig. 9 (left), at constant temperature $T = 420$ K the mixture occurs in two-phase from the lowest molar densities up to approximately 6.5 kmol m^{-3}, then it becomes single-phase.

The equilibrium pressure as a function of the overall molar density c is presented in Fig. 9 (right) illustrating a steady rise of the equilibrium pressure during compression, and a substantial

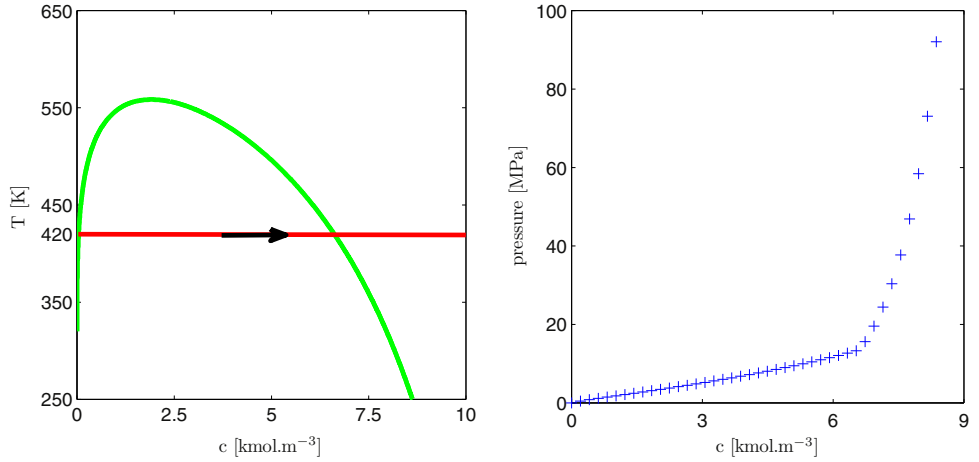

Fig. 9. Approximate boundary between the single-phase and two-phase domains in the c, T-space (left). The arrow indicates the compression at constant temperature $T = 420$ K. The equilibrium pressure as a function of the overall molar density c at $T = 420$ K (right). Example 4: ternary C_1–C_6–nC_{10} mixture ($z_{C_1} = 0.405946$, $z_{C_6} = 0.297027$, $z_{C_{10}} = 0.297027$).

Table 3
Binary interaction coefficients for the ternary mixture used in Example 4.

Component	C_1	C_6	nC_{10}
C_1	0	0.043	0.052
C_6	0.043	0	0
nC_{10}	0.052	0	0

Table 4
Binary interaction coefficients for the four-component mixture used in Example 5.

Component	N_2	C_1	C_3	nC_{10}
N_2	0	0.1	0.1	0.1
C_1	0.1	0	0.036	0.052
C_3	0.1	0.036	0	0
nC_{10}	0.1	0.052	0	0

increase at molar densities 6.5 kmol m^{-3} and higher when all gas phase is depleted. Saturations of both phases and mass densities of both phases as functions of the overall molar density c are presented in Fig. 10. Mole fractions of all components in both phases as functions of the overall molar density c are presented in Fig. 11.

Example 5

In the fifth example, we investigate phase equilibrium for a four-component mixture of nitrogen (N_2), methane (C_1), propane (C_3), and normal decane (nC_{10}) with mole fractions $z_{N_2} = 0.2463$, $z_{C_1} = 0.2208$, $z_{C_3} = 0.2208$, and $z_{nC_{10}} = 0.3121$. The binary interaction coefficients are shown in Table 4. The approximate boundary between the single-phase and two-phase domains in the c, T-space obtained from VT-stability analysis is shown in Fig. 12 (left). As shown in Fig. 12 (left), at constant temperature $T = 393.15$ K the mixture occurs in two-phase from the lowest molar densities up to approximately 8.2 kmol m^{-3}, then it becomes single-phase.

The equilibrium pressure as a function of the overall molar density c is presented in Fig. 12 (right) illustrating a steady rise of the equilibrium pressure during compression, and a substantial increase at molar densities 8.2 kmol m^{-3} and higher when the gas phase is depleted. Saturations of both phases and mass densities of both phases as functions of the overall molar density c are presented in Fig. 13. Mole fractions of all components in both phases as functions of the overall molar density c are presented in Fig. 14.

Example 6

In the sixth example, we investigate phase equilibrium for a binary mixture of water (H_2O) and carbon dioxide (CO_2) with mole fractions $z_{H_2O} = 0.5$ and $z_{CO_2} = 0.5$. The binary interaction

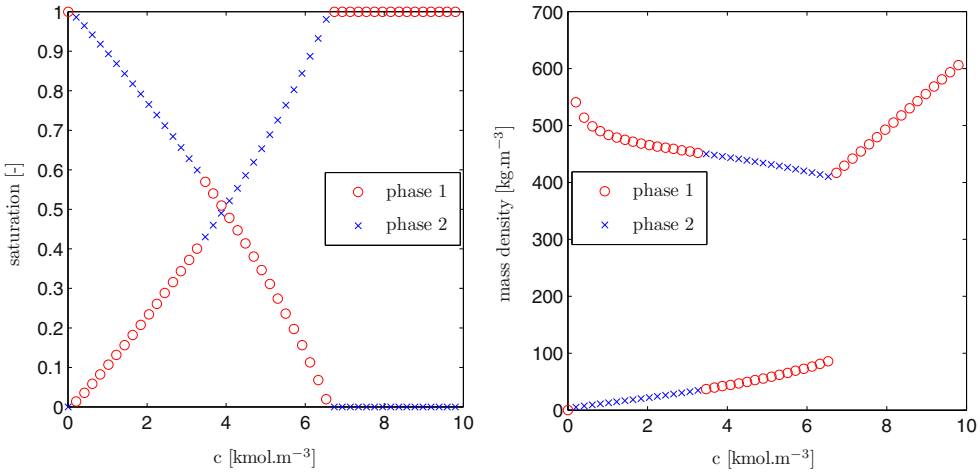

Fig. 10. Saturations (left) and mass densities of both phases (right) as functions of the overall molar density c. Example 4: ternary C_1–C_6–nC_{10} mixture ($z_{C_1} = 0.405946$, $z_{C_6} = 0.297027$, $z_{C_{10}} = 0.297027$, and $T = 420$ K).

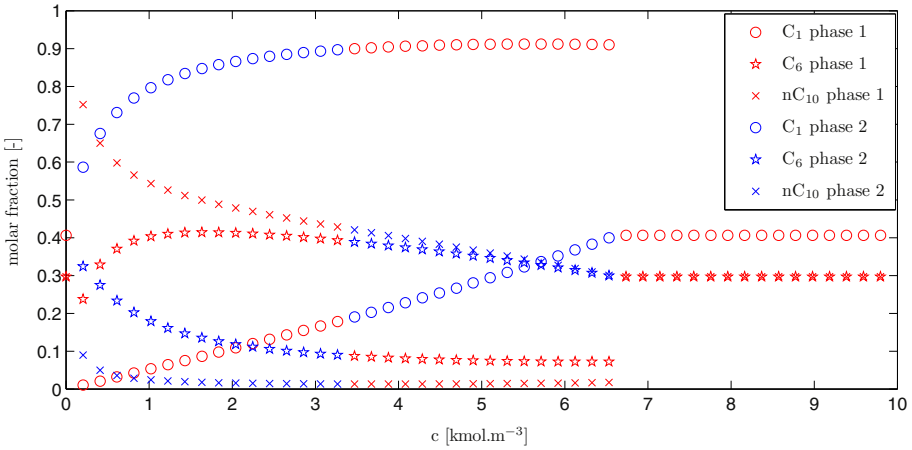

Fig. 11. Molar fractions of all components in both phases as functions of the overall molar density c at $T = 420$ K. Example 4: ternary C_1–C_6–nC_{10} mixture ($z_{C_1} = 0.405946$, $z_{C_6} = 0.297027$ and $z_{C_{10}} = 0.297027$).

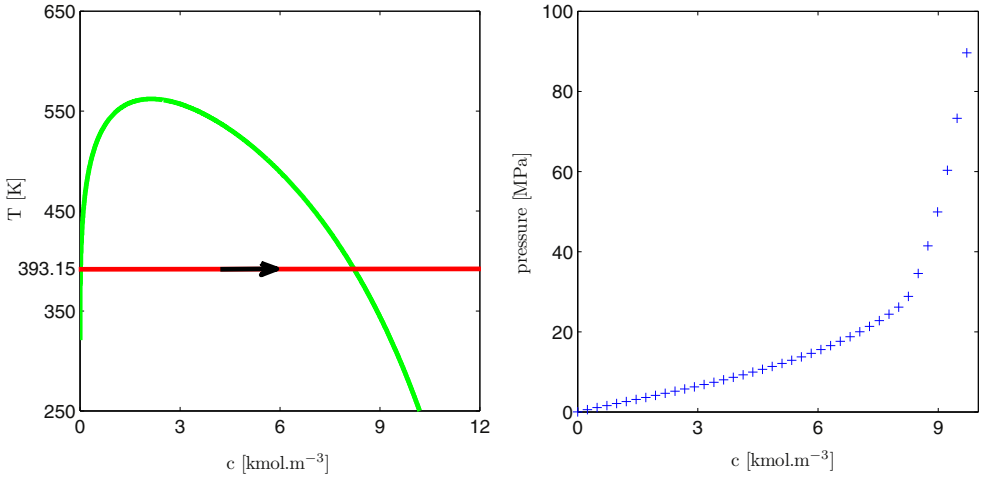

Fig. 12. Approximate boundary between the single-phase and two-phase domains in the c, T-space (left). The arrow indicates the compression at constant temperature $T = 393.15$ K. Equilibrium pressure as a function of the overall molar density c at $T = 393.15$ K (right). Example 5: mixture of N_2–C_1–C_3–nC_{10} ($z_{N_2} = 0.2463$, $z_{C_1} = 0.2208$, $z_{C_3} = 0.2208$, $z_{nC_{10}} = 0.3121$).

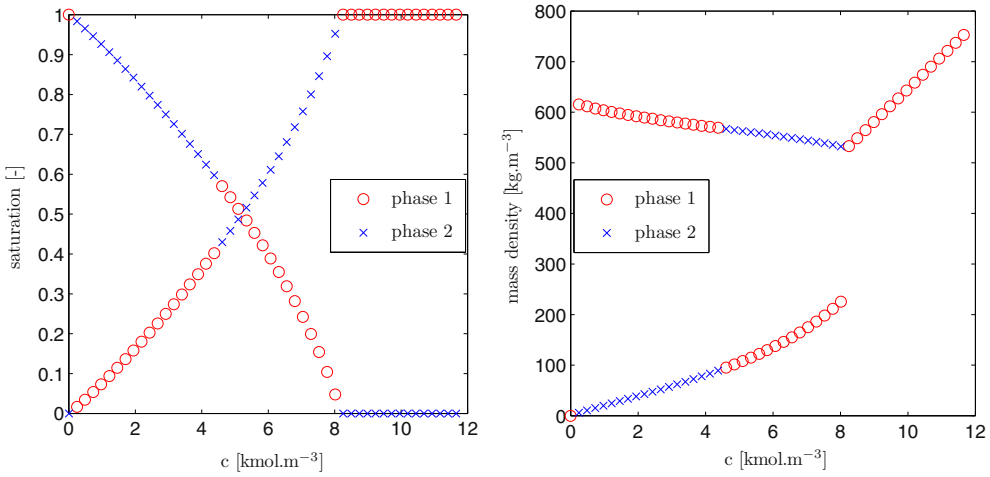

Fig. 13. Saturations (left) and mass densities (right) of both phases as functions of the overall molar density c (right). Example 5: four-component mixture of N_2–C_1–C_3–nC_{10} ($z_{N_2} = 0.2463$, $z_{C_1} = 0.2208$, $z_{C_3} = 0.2208$, $z_{nC_{10}} = 0.3121$, and $T = 393.15$ K).

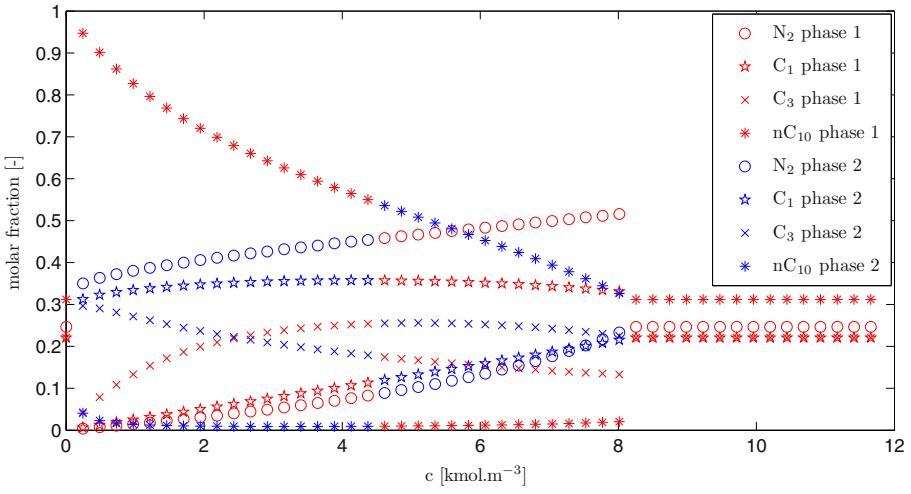

Fig. 14. Molar fractions of all components in both phases as functions of the overall molar density c at $T = 393.15$ K. Example 5: mixture of four-components N_2–C_1–C_3–nC_{10} ($z_{N_2} = 0.2463$, $z_{C_1} = 0.2208$, $z_{C_3} = 0.2208$, $z_{nC_{10}} = 0.3121$).

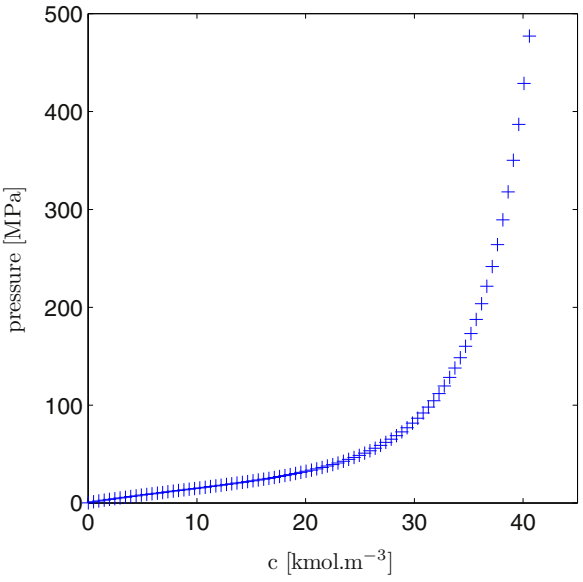

Fig. 15. Equilibrium pressure as a function of the overall molar density c at $T = 413.15$ K. Example 6: binary H_2O–CO_2 mixture ($z_{H_2O} = 0.5$, $z_{CO_2} = 0.5$).

coefficient $\delta_{H_2O-CO_2} = 0.30544$ (for temperature $T = 413.15$ K). The cross association factor used in the CPA equation of state is $s_{CO_2} = 0.083196882$ (for temperature $T = 413.15$ K). As $\delta_{H_2O-CO_2}$ and s_{CO_2} are strongly dependent on temperature, we omit the computation of the stability region for this mixture. For $T = 413.15$ K, the mixture splits in two phases except from very low overall concentrations c.

The equilibrium pressure as a function of the overall molar density c is presented in Fig. 15 (right) illustrating a steady increase of the equilibrium pressure during compression. Saturations of both phases and mass densities of both phases as functions of the overall molar density c are presented in Fig. 16. Mole fractions of both components in both phases as functions of the overall molar density c are presented in Fig. 17. Unlike in previous Examples, we see that the mutual solubility of CO_2 and water is limited.

7. Summary and conclusions

In this work, we have developed a numerical algorithm for the calculation of two-phase equilibria at constant volume, temperature, and moles. The algorithm uses the Newton–Raphson method with line-search for the minimization of the total Helmholtz free energy A of the mixture. The modified Cholesky decomposition of the Hessian matrix ensures the decrease of A in every iteration. The initial guess is constructed using the results of the VT-stability

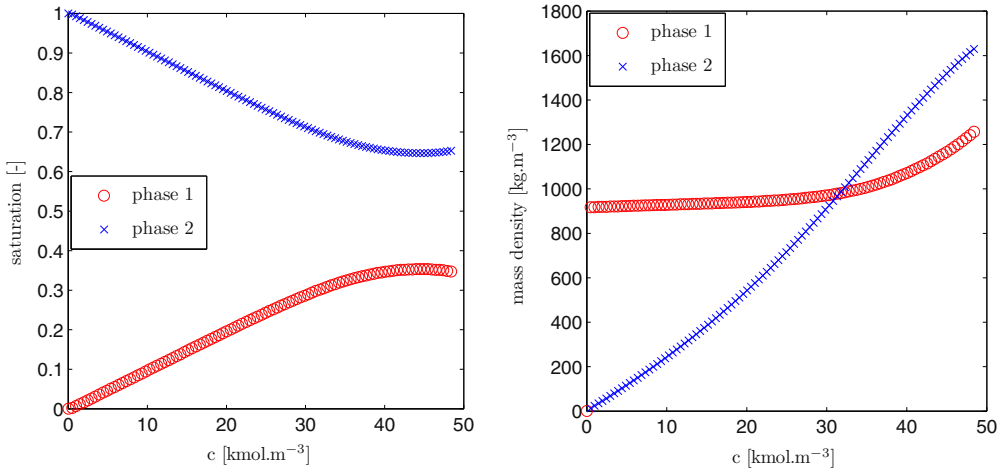

Fig. 16. Saturations (left) and mass densities (right) of both phases as functions of the overall molar density c (right). Example 6: binary H_2O–CO_2 mixture ($z_{H_2O} = 0.5$, $z_{CO_2} = 0.5$, and $T = 413.15$ K).

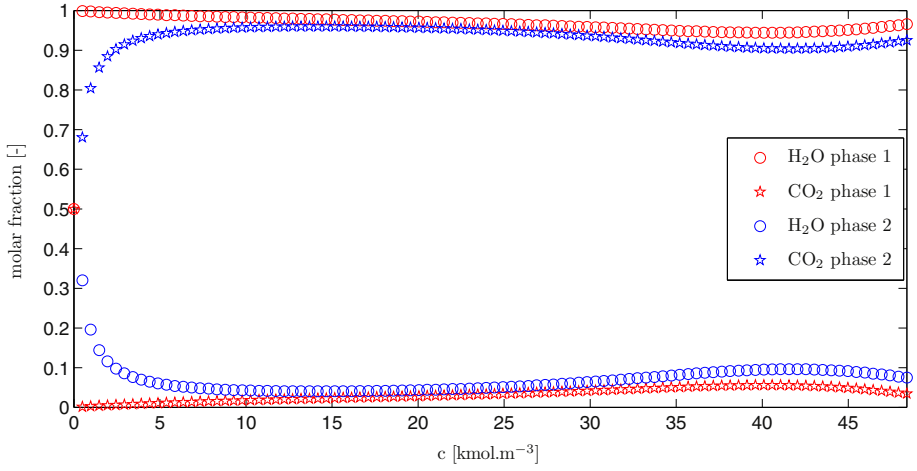

Fig. 17. Molar fractions of both components in both phases as functions of the overall molar density c at $T = 413.15$ K. Example 6: binary H_2O–CO_2 mixture ($z_{H_2O} = 0.5$, $z_{CO_2} = 0.5$).

testing. This approach guarantees that the algorithm always converges to a state of local minimum of A and the possibility of convergence towards the trivial solution is avoided. Compared to the SSI method developed previously in [9], the new algorithm is fast – usually it converges in 6–10 iterations. We have not encountered a case in which the algorithm would not converge. The robustness of our algorithm is documented by the numerous examples provided in this paper. The algorithm was tested on many hydrocarbon mixtures that were described using the Peng–Robinson equation of state and on the H_2O–CO_2 mixture described by the CPA equation of state. We believe that the same approach will be useful for other pressure-explicit equations of state as well.

Acknowledgements

The work was supported by the projects LH12064 Computational Methods in Thermodynamics of Hydrocarbon Mixtures of the Ministry of Education of the Czech Republic, P105/11/1507 Development of Computer Models of CO_2 Sequestration in the Subsurface of the Czech Science Foundation, by the research direction project MSM6840770010 Applied Mathematics in Technical and Physical Sciences of the Ministry of Education of the Czech Republic, and by the project SGS11/161/OHK4/3T/14 Advanced Supercomputing Methods for Implementation of Mathematical Models of the Student Grant Agency of the Czech Technical University in Prague.

Appendix A. Equations of state

In this work we use in Examples 1–5 the Peng–Robinson equation of state [14] in the form

$$P(V,T,N_1,\dots,N_n)=\frac{NRT}{V-\mathcal{B}}-\frac{\mathcal{A}}{V^2+2\mathcal{B}V-\mathcal{B}^2},$$

where R is the universal gas constant, $N=\sum_{i=1}^{n}N_i$ is the total mole number, and coefficients $\mathcal{A}$ and $\mathcal{B}$ are given by

$$\mathcal{A}=\sum_{i=1}^{n}\sum_{j=1}^{n}N_iN_ja_{ij},$$

$$\mathcal{B}=\sum_{i=1}^{n}N_ib_i,$$

$$a_{ij}=(1-\delta_{i-j})\sqrt{a_ia_j},$$

$$b_i=0.0778\frac{RT_{i,crit}}{P_{i,crit}},$$

$$a_i=0.45724\frac{R^2T_{i,crit}^2}{P_{i,crit}}\left[1+m_i\left(1-\sqrt{T_{r,i}}\right)\right]^2,$$

$$T_{r,i}=\frac{T}{T_{i,crit}},$$

$$m_i=\begin{cases}0.37464+1.54226\omega_i-0.26992\omega_i^2,\\ \text{for } \omega_i<0.5,\\ \\ 0.3796+1.485\omega_i-0.1644\omega_i^2+0.01667\omega_i^3,\\ \text{for } \omega_i\geq 0.5.\end{cases}$$

In these equations δ_{i-j} denotes the binary interaction parameter between the components i and j, $T_{i,crit}$, $P_{i,crit}$, and ω_i are the critical temperature, critical pressure, and accentric factor of the ith component, respectively.

In Example 6 we use for the binary mixture of water (H_2O) and carbon dioxide (CO_2) the Cubic-Plus-Association (CPA) equation of state [15,16]. This equation uses the Peng–Robinson equation of state for the physical interactions and the termodynamic perturbation theory for the bonding of water molecules. We assume that each water molecule has four association sites of two types (mark them α and β), so each type has two sites. We assume the same for each molecule of carbon dioxide, whose association sites can be marked as α' and β'. Let χ_α and χ_β be the mole fractions of water not bonded at site α and β, respectively, and let $\chi_{\alpha'}$ and $\chi_{\beta'}$ be the mole fractions of carbon dioxide not bonded at site α' and β', respectively. Assuming neither cross association nor self association between carbon dioxide molecules, and symmetric cross association between the two sites of different type of water and carbon dioxide, we obtain the following simplified expressions for the symmetric association model

$$\chi_\alpha=\chi_\beta=\chi_w=\frac{1}{1+2(N_w/V)\chi_w\Delta^{\alpha\beta}+2(N_c/V)\chi_c\Delta^{\alpha\beta'}},$$

$$\chi_{\alpha'}=\chi_{\beta'}=\chi_c=\frac{1}{1+2(N_w/V)\chi_c\Delta^{\alpha\beta'}}.$$

In these equations the association strength between molecules of water is given by

$$\Delta^{\alpha\beta}=g\kappa^{\alpha\beta}[\exp(\varepsilon^{\alpha\beta}/k_BT)-1],$$

where k_B is the Boltzmann constant, $\kappa^{\alpha\beta}$ and $\varepsilon^{\alpha\beta}$ are the bonding volume and energy parameters of water, respectively, and g is the contact value of the radial distribution function of hard-sphere mixture that can be approximated as $g=g(\eta)\approx(1-0.5\eta)/(1-\eta)^3$, where $\eta=\mathcal{B}/(4V)$. The association strength between water and carbon dioxide molecules is related to the strength between water molecules as $\Delta^{\alpha\beta'}=s_i\Delta^{\alpha\beta}$ where s_i is the temperature-dependent cross association coefficient which can be determined together with the binary interaction coefficient by fitting the experimental data. As a result, the CPA equation of state for the binary mixture of water and carbon dioxide is given by

$$P(V,T,N_w,N_c)=\frac{NRT}{V-\mathcal{B}}-\frac{\mathcal{A}}{V^2+2\mathcal{B}V-\mathcal{B}^2}+2RT\left(\frac{\eta}{g}\frac{\partial g}{\partial\eta}+1\right)\times\left[\frac{N_w}{V}(\chi_w-1)+\frac{N_c}{V}(\chi_c-1)\right],$$

where R, $\mathcal{A}$ and $\mathcal{B}$ are the parameters from the Peng–Robinson equation of state, N_w and N_c are the mole numbers of water and carbon dioxide, $N=N_w+N_c$, and $\partial g/\partial\eta=(2.5-\eta)/(1-\eta)^4$. The coefficients a_i and b_i for water read as $a_w=a_w^0[1.0+c_1(1-\sqrt{T_{r,w}})+c_2(1-\sqrt{T_{r,w}})^2+c_3(1-\sqrt{T_{r,w}})^3]^2$, $b_w=1.458431489141052\cdot10^{-5}$, where a_w^0, c_1, c_2, c_3 are the parameters of the equation of state given in Table 5.

Table 5
Parameters of the CPA equation of state for the H_2O and CO_2 mixture (the notation is explained in Appendix A).

Symbol	Units	Value
$\kappa^{\alpha\beta}$	[m^3 mol^{-1}]	$1.801506043021089\times10^{-6}$
$\varepsilon^{\alpha\beta}/k_B$	[K]	1738.393603227767
a_w^0	[J m^{-3} mol^{-2}]	0.09627316625476
c_1	–	1.75573246325004
c_2	–	0.00351802110081
c_3	–	−0.27463687473246

References

[1] M.L. Michelsen, Fluid Phase Equilib. 9 (1982) 1–19.
[2] M.L. Michelsen, J.M. Mollerup, Thermodynamic Models: Fundamentals and Computational Aspects, Tie-Line Publications, 2004.
[3] M.L. Michelsen, Fluid Phase Equilib. 9 (1982) 21–40.
[4] M.L. Michelsen, Fluid Phase Equilib. 158 (1999) 617–626.
[5] R.O. Espósito, M. Castier, F.W. Tavares, Chem. Eng. Sci. 55 (2000) 3495–3504.

[6] M. Castier, F.W. Tavares, Chem. Eng. Sci. 60 (2005) 2927–2935.
[7] V.F. Cabral, M. Castier, F.W. Tavares, Chem. Eng. Sci. 60 (2005) 1773–1782.
[9] J. Mikyška, A. Firoozabadi, AIChE J. 57 (2011) 1897–1904.
[10] J. Mikyška, A. Firoozabadi, Fluid Phase Equilib. 321 (2012) 1–9.
[11] S.E. Qui nones-Cisneros, U.K. Deiters, Fluid Phase Equilib. 329 (2012) 22–31.
[12] P.E. Gill, W. Murray, M.H. Wright, Practical Optimization, Academic Press, 1997.
[13] A. Quaternioni, R. Sacco, F. Saleri, Numerical Mathematics, Springer, 2000.
[14] D.E. Peng, D.B. Robinson, Ind. Eng. Chem.: Fundam. 15 (1976) 59–64.
[15] A. Firoozabadi, Thermodynamics of Hydrocarbon Reservoirs, McGrew-Hill, 1999.
[16] Z. Li, A. Firoozabadi, AIChE J. 55 (7) (2009) 1803–1813.